

## FULL ARTICLE

# Correcting the limited view in optical-resolution photoacoustic microscopy

Wei Liu<sup>1</sup> | Yuan Zhou<sup>1,2</sup> | Mengran Wang<sup>3</sup> | Lei Li<sup>4</sup> | Emelina Vienneau<sup>1</sup> | Ruimin Chen<sup>5</sup> | Jianwen Luo<sup>2</sup> | Chris Xu<sup>3</sup> | Qifa Zhou<sup>5</sup> | Lihong V. Wang<sup>4</sup> | Junjie Yao<sup>1\*</sup>

<sup>1</sup>Department of Biomedical Engineering, Duke University, Durham, North Carolina

<sup>2</sup>Department of Biomedical Engineering, School of Medicine, Tsinghua University, Beijing, China

<sup>3</sup>School of Applied and Engineering Physics, Cornell University, Ithaca, New York

<sup>4</sup>Caltech Optical Imaging Laboratory, Andrew and Peggy Cherng Department of Medical Engineering, Department of Electrical Engineering, California Institute of Technology, Pasadena, California

<sup>5</sup>Department of Biomedical Engineering, University of Southern California, Los Angeles, California

**\*Correspondence**

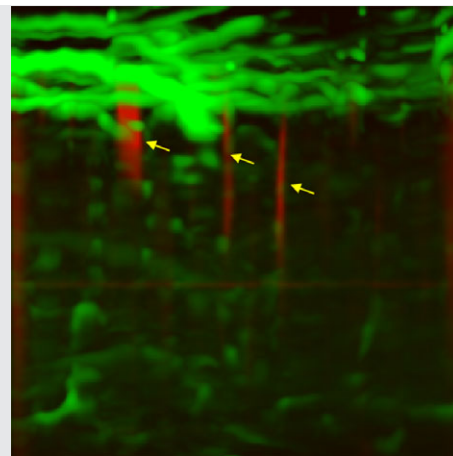
Junjie Yao, Department of Biomedical Engineering, Duke University, Durham, NC 27708.

Email: junjie.yao@duke.edu

**Funding information**

Duke MEDx

Optical-resolution photoacoustic microscopy (OR-PAM) has proven useful for anatomical and functional imaging with high spatial resolutions. However, the coherent signal generation and the desired reflection-mode detection in OR-PAM can result in a limited detectability of features aligned with the acoustic axis (ie, vertical structures). Here, we investigated the limited-view phenomenon in OR-PAM by simulating the generation and propagation of the acoustic pressure waves and determined the key optical parameters affecting the visibility of vertical structures. Proof-of-concept numerical experiments were performed with different illumination angles, optical foci and numerical apertures (NA) of the objective lens. The results collectively show that an NA of 0.3 can readily improve the visibility of vertical structures in a typical reflection-mode OR-PAM system. This conclusion was confirmed by numerical simulations on the cortical blood vessels in a mouse brain and by experiments in a suture-cross phantom and in a mouse brain in vivo.

**KEYWORDS**

coherent signal, *K*-wave, limited view, mouse brain, photoacoustic imaging

## 1 | INTRODUCTION

Photoacoustic tomography (PAT) [1, 2] is a complementary imaging modality to other existing biomedical optical imaging techniques such as optical coherence tomography [3] and 2-photon microscopy [4] and has been proven effective in structural [5], functional [6, 7] and molecular [8] imaging in vivo. PAT has 2 major implementations [1]: Photoacoustic computed tomography (PACT) and photoacoustic microscopy (PAM). The difference between the 2 implementations lies largely in the optical illumination and

acoustic detection strategies. PACT usually employs wide-field optical illumination and parallel acoustic detection, covering a relatively large field of view. It is known that a typical PACT configuration with a linear transducer array has a limited-view phenomenon due to the coherent signal generation [9, 10] in which the linear transducer array cannot receive the photoacoustic (PA) waves generated by the absorbing structures aligned with the norm of the transducer array surface. This limited-view phenomenon results in missing vertical structures in the reconstructed PA image and may lead to misinterpretation of the results. Several

methods based on dynamic speckle illumination [11], acoustic reflectors [12] and thermal nonlinearity [13] have been published for improving the visibility of vertical structures under respective applicable conditions. Conversely, PAM, especially optical-resolution photoacoustic microscopy (OR-PAM), applies focused optical illumination and/or acoustic detection and achieves a much higher spatial resolution than PACT at the cost of maximum penetration depth. It is typically assumed that OR-PAM is not subject to the limited-view problem due to the spatially confined optical illumination. However, this is a misconception because the acoustic wavelength in OR-PAM is usually comparable to or even smaller than the optical focal zone and thus the effective target along the acoustic axis cannot always be treated as a point source emitting spherical acoustic waves. For example, in a typical OR-PAM setup, the depth of focus (DOF) or optical focal zone is about 60  $\mu\text{m}$  (objective lens' numerical apertures (NA): 0.1), while the acoustic wavelength is about 30  $\mu\text{m}$  (transducer's central frequency: 50 MHz) [14]. In this case, the acoustic wavelength is shorter than the optical DOF. When the target happens to be a vertical structure, the illuminated region is effectively a cylindrically shaped acoustic source that emits cylindrical acoustic waves, which propagate in the direction perpendicular to the transducer's acoustic axis, while the acoustic waves propagating along the transducer's acoustic axis are largely canceled out. In this case, OR-PAM does have a limited visibility of vertical structures (such as penetrating pia vessels in the mouse brain). This becomes even more evident in OR-PAM using high-frequency ultrasound detection [15]. It is worth noting that the acoustic DOF, which is on the level of hundreds of micrometers, only affects the overall detected signal strength and does not contribute to the limited view problem of OR-PAM. In this paper, we aim to clarify the limited-view phenomenon in OR-PAM and provide a simple solution for improvement.

## 2 | MATERIALS AND METHODS

A typical reflection-mode OR-PAM setup is shown in Figure 1. A collimated laser beam is focused by an objective lens and illuminates the sample. The sample is placed on a 3-axis motor scanning stage. An ultrasonic transducer (central frequency: 50 MHz) with a concave acoustic lens detects the time-resolved acoustic pressure at each scanning position. The ultrasound transducer is confocally aligned with the laser beam via an acoustic-optical beam combiner, as described in a previous publication [14]. The length of the beam combiner is around 1 cm. With the additional acoustic focal length of at least 6 mm, the working distance for the objective lens should be at least 1.6 cm. The need for such a long working distance leads to the common practice of using a low-NA ( $\sim 0.1$ ) objective lens to focus the

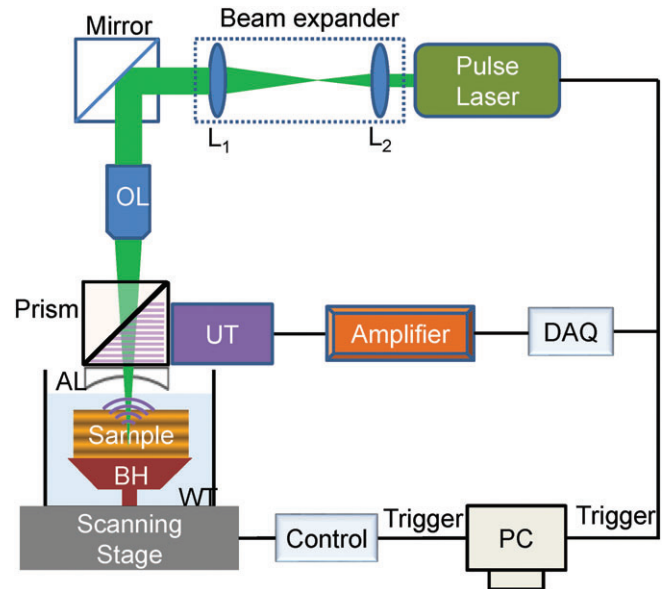


**FIGURE 1** Schematic of a representative reflection-mode OR-PAM setup with a low-NA objective lens, showing the long working distance required by the acoustic-optical beam combiner. AL, acoustic lens; BH, bench hook; DAQ, data acquisition;  $L_1$  and  $L_2$ , convex lenses; OL, objective lens; PC, computer; UT, ultrasonic transducer; WT, water tank

optical beam in most OR-PAM systems. It becomes increasingly challenging to use objective lenses with higher NAs in reflection-mode OR-PAM [16, 17], although novel designs have been reported with more complicated acoustic-optical combining methods [17].

The limited-view phenomenon in OR-PAM originates from the coherent generation of acoustic pressure waves. For simplicity, we assume the laser pulse width satisfies both the thermal and stress confinements [1]. At each scanning position, the amplitude of the initial acoustic pressure rise upon optical excitation at the position  $(x, y, z)$  is [18]

$$P(x, y, z) = \Gamma \eta \mu_a(x, y, z) F(x, y, z), \quad (1)$$

where  $\Gamma$  is the Grüneisen parameter (dimensionless),  $\eta$  is the percentage of absorbed light energy that is converted into heat through non-radiative relaxation,  $\mu_a(x, y, z)$  is the absorption coefficient ( $\text{cm}^{-1}$ ) and  $F(x, y, z)$  is the local light fluence ( $\text{J cm}^{-2}$ ).  $F(x, y, z)$  can be estimated as a Gaussian beam in space and is expressed as

$$F(x, y, z) = F_0 \left[ \omega_0 / \omega(z) \right]^2 \exp \left[ -2(x^2 + y^2) / \omega(z)^2 \right], \quad (2)$$

where  $F_0$  is the maximum central fluence at the focal point,  $\omega_0$  is the waist radius and  $\omega(z)$  is the beam spot size at  $z$ . For simplicity, both absorption and scattering effects on beam propagation are neglected here. We would like to point out that the optical attenuation can also induce reduced visibility of the vertical structures in OR-PAM as it prevents light going deeper along the vertical structures. However, such an optical-attenuation-induced limited view

can happen to any types of optical microscopy, which is often referred to as the “optical shadowing effect,” while the coherent-signal-interference-induced limited view can happen only to OR-PAM.

Given the objective lens’ NA,  $F(x, y, z)$  can be rewritten as [19]

$$F(x, y, z) \approx \frac{F_0 \lambda^2}{\lambda^2 + z^2 \pi^2 \text{NA}^4} \exp \left[ -\frac{2(x^2 + y^2) \pi^2 \text{NA}^2}{\lambda^2 + z^2 \pi^2 \text{NA}^4} \right]. \quad (3)$$

Therefore, Eq. (1) can be rewritten as

$$P(x, y, z) \approx \frac{\Gamma F_0 \lambda^2 \mu_a(x, y, z)}{\lambda^2 + z^2 \pi^2 \text{NA}^4} \exp \left[ -\frac{2(x^2 + y^2) \pi^2}{\lambda^2 / \text{NA}^2 + z^2 \pi^2 \text{NA}^2} \right]. \quad (4)$$

Equation (4) shows that the initial pressure distribution  $P(x, y, z)$  mostly depends on the optical wavelength  $\lambda$ , the absorption coefficient distribution  $\mu_a(x, y, z)$  and the objective lens’ NA. Generally, the optical wavelength  $\lambda$  is a constant. The contribution of  $\mu_a(x, y, z)$  to the pressure distribution is also minimized when imaging a relatively large and homogenous target. As a result, NA is the primary factor that determines the initial pressure distribution. In other words, the initial pressure rise in OR-PAM reflects the original optical energy deposition in the target, which is mostly determined by the shape of the focused optical beam.

The coherent superposition of the PA pressure waves generated by a homogeneous absorbing medium (such as blood) results in a “boundary buildup effect,” leading to a wave propagation pattern following the target’s shape [10]. This effect is the fundamental cause of the limited-view phenomenon in PACT, and the same principle also applies in OR-PAM. According to Eq. (4), it is expected that the distribution of  $P(x, y, z)$  is largely shaped by the objective lens’ NA. Therefore, a relatively small NA (eg, 0.1) results in a slowly changing optical fluence and an accordingly similar pressure distribution along the acoustic axis, causing the acoustic pressure waves to propagate more like cylindrical waves rather than the expected spherical waves. Most of the waves propagate in the direction perpendicular to the acoustic axis and thus cannot reach the ultrasonic transducer, which leads to the limited-view phenomenon in OR-PAM.

### 3 | RESULTS AND DISCUSSION

To validate the above theory, proof-of-concept investigations were carried out using numerical simulations based on the *K*-wave toolbox [20, 21] with various optical illumination parameters while the wavelength of the laser beam was set to 532 nm. First, we simulated the received raw PA

signals based on a 0.1-NA objective lens. The optical fluence has a Gaussian distribution, as indicated by Eq. (2). The target was a homogeneous T-shaped absorber composed of 2 orthogonal bars with a width of 30  $\mu\text{m}$  and a length of 50  $\mu\text{m}$ . The size of the bars was chosen to match the optical absorption length at 532 nm in penetrating blood vessels. The absorption coefficient of the T-shaped bar is  $1 \text{ cm}^{-1}$ , so the optical attenuation inside the bars can be neglected. To reduce the simulation time, we placed the transducer 300  $\mu\text{m}$  away from the laser beam’s focal point. The transducer’s center frequency and bandwidth are both 50 MHz. A high-frequency ultrasound transducer is used here to better illustrate the limited-view phenomenon in OR-PAM because a higher ultrasound frequency (ie, a shorter acoustic wavelength) should result in a more significant limited view [15, 22]. The ultrasonic transducer receives the time-resolved A-line signals with a typical bipolar characteristic along the acoustic axis. We scanned the sample with a step size of 1  $\mu\text{m}$ . Cross-sectional B-scan images were obtained by stacking the raw A-line signals. Here, we show the raw radio-frequency data to better illustrate the boundary-buildup effect [23].

The T-shaped target used in the simulation is shown in Figure 2A.  $\theta$  is the illumination/detection angle, defined as the clockwise angle from the  $z$  axis to the incident beam direction (ie, the acoustic axis). Figure 2B-D shows the corresponding B-scan images taken at 3 different illumination angles:  $0^\circ$ ,  $90^\circ$  and  $180^\circ$ , respectively. For  $0^\circ$  illumination, the scanning direction of the optical focus was along the central line of the horizontal bar and the optical beam illuminated the target from the top as shown in Figure 2B. This result shows that the acoustic pressure waves only from the horizontal boundaries of the T-bar are visible, whereas signals from the top and bottom boundaries are visible but have opposite signs. The signal from the bottom boundary is weaker than that from the top boundary due to acoustic divergence. The vertical bar is entirely invisible, which is consistent with our theory above that most of the signals propagate perpendicular to the axial axis. Similarly, for  $90^\circ$  illumination, the scanning direction was along the long central line of the vertical bar and the beam illuminated the target from the right as shown in Figure 2C. In this case, the pressure waves only from the left and right vertical edges are visible, but the pressure waves from the horizontal boundaries are invisible. This result further confirms the limited-view phenomenon in OR-PAM. Finally, Figure 2D shows the case of illuminating the target from the bottom. The scanning was along the short central line of the vertical bar. The limited-view problem still exists because only the pressure from the horizontal boundaries is visible, like the first case.

Collectively, the results in Figure 2 demonstrate that the limited-view phenomenon exists in OR-PAM with a small-NA objective. This problem can affect the quality of the

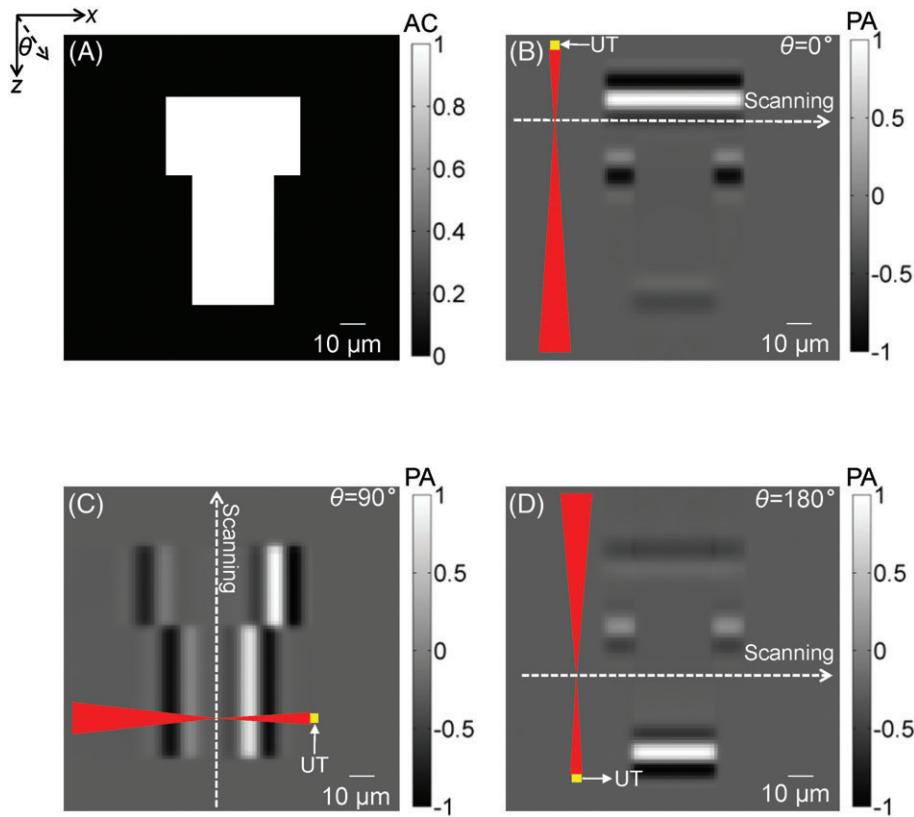


**FIGURE 2** Numerical simulations of the visibility of a T-shaped target with different illumination/detection angles, based on a 0.1-NA objective lens. (A) Optical absorption of the T-shaped target. AC, absorption coefficient ( $\text{cm}^{-1}$ );  $\theta$ , illumination/detection angle. (B) Simulated raw B-scan image obtained with an illumination angle of  $0^\circ$ . PA, normalized pressure amplitude. The focal point of the optical beam was scanned along the long central line of the horizontal bar. Note the bipolar nature of the raw PA signals. (C) B-scan image obtained with an illumination angle of  $90^\circ$ . The laser focal point was scanned along the long central line of the vertical bar. (D) B-scan image obtained with an illumination angle of  $180^\circ$ . Focal point was scanned along the short central line of the vertical bar

final tomographic image since the vertical boundaries can be completely lost. For example, when imaging the cortical blood vessels in a mouse brain, the penetrating pia microvessels (diameters: 10 to 50  $\mu\text{m}$ ; length:  $\sim 100 \mu\text{m}$ ) will likely be invisible.

One straightforward solution to mitigate the limited-view problem is to reduce the homogeneity of the optical

fluence along the acoustic axis. Compared to the solutions for PACT [11–13], an easier way for OR-PAM is to increase the objective NA, which can effectively shorten the DOF of the optical beam ( $\text{DOF} \propto 1/\text{NA}^2$ ). To investigate the effect of the objective NA on the visibility of vertical structures, numerical simulations were performed by imaging the same T-shaped target with 4 representative objective

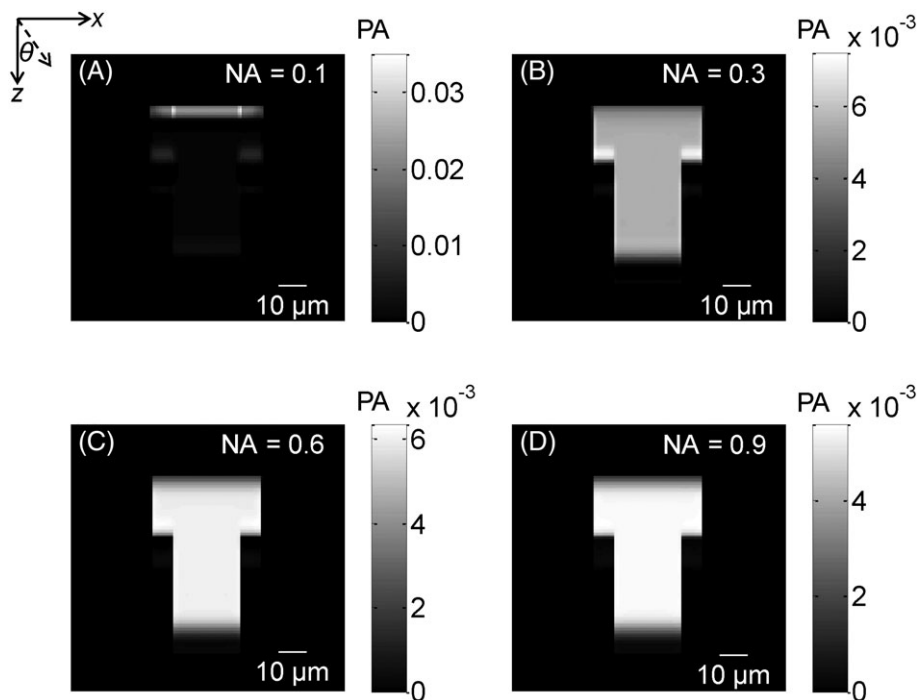


**FIGURE 3** Simulated composite B-scan PA images showing the visibility of the T-shaped target with different objective NAs of (A) 0.1, (B) 0.3, (C) 0.6 and (D) 0.9

**TABLE 1** Visibility of the vertical bar with different objective NAs

NA	0.1	0.2	0.3	0.6	0.9
DOF ( $\mu\text{m}$ )	60.28	15.07	6.70	1.67	0.74
$V$	0.20	0.80	0.91	0.97	0.97

NAs (0.1, 0.3, 0.6 and 0.9) with both  $x$ - and  $z$ -axis scanning. These 4 objectives were chosen due to their wide availability in optical imaging. The scanning step sizes for the 4 cases along both  $x$  axis and  $z$  axis were all 1  $\mu\text{m}$ . The illumination/detection angle is  $0^\circ$ , mimicking the typical reflection-mode configuration in OR-PAM. A composite B-scan image was obtained by overlaying the individual B-scan images at different  $z$  scanning positions. The composite B-scan images with different objective NAs are shown in Figure 3. The results clearly show that the visibility of the vertical structures is significantly improved with NAs of 0.3, 0.6 and 0.9.

Here, we define the visibility of the vertical structure of the T-shaped target as

$$V = \frac{\overline{\sum P_v(x, y, z)}}{\overline{\sum P_h(x, y, z)}}, \quad (5)$$

where  $\overline{\sum P_v(x, y, z)}$  denotes the mean signal amplitude of the vertical bar and  $\overline{\sum P_h(x, y, z)}$  indicates the mean signal amplitude of the horizontal bar. The DOFs and the  $V$  values with different objective NAs are summarized in Table 1. As the 0.1-NA objective has the largest DOF, it results in the worst visibility of the vertical bar. The visibility is increased significantly from 0.1 to 0.3 NA and slightly increased from 0.3 to 0.9 NA, showing that a 0.3 NA is sufficient to correct

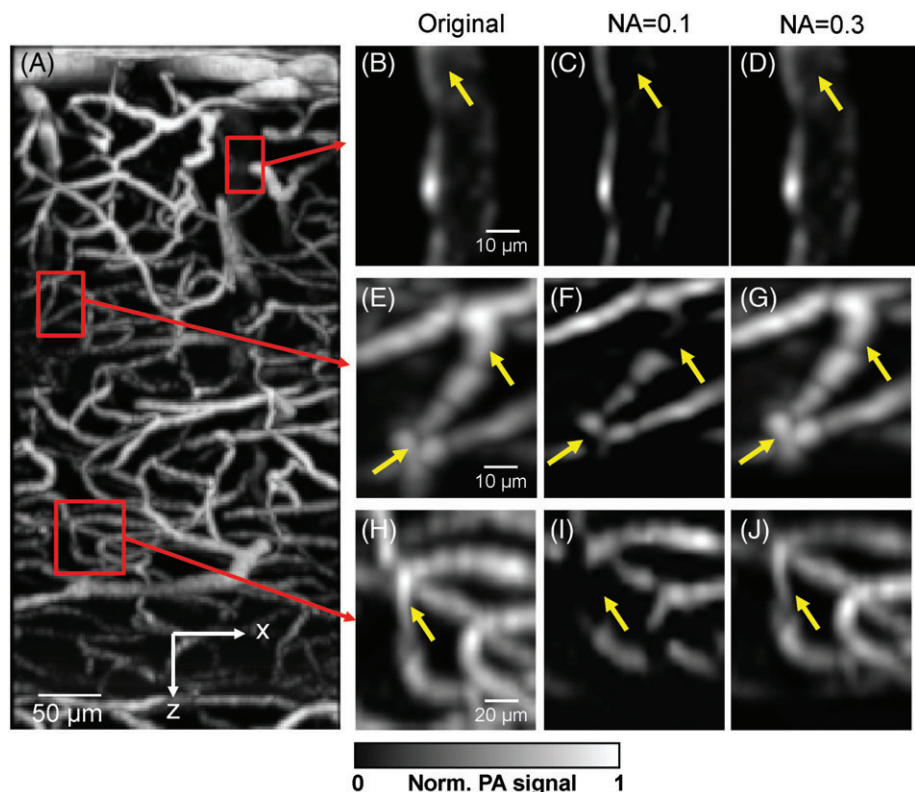
the limited-view phenomenon in OR-PAM. We also simulated the visibility by using a 0.2-NA objective, as shown in Table 1, which, however, is not commonly available in OR-PAM.

The numerical simulation results in Figure 3 strongly suggest that the limited-view effect in OR-PAM can be suppressed by using a large-NA objective. The drawback is that a large NA (especially  $\geq 0.6$ ) leads to a short working distance due to the short optical focal length, a relatively short penetration depth due to the longer light path length, and the requirement of axial scanning due to the short optical DOF. Consequently, there is a trade-off between the visibility of vertical structures and the operating space and convenience of the imaging system, implying that the choice of NA depends on the application. Our simulation results show that the widely available 0.3-NA objective is sufficient to image the vertical structures while still maintaining a relatively long working distance and a maximum penetration depth than other higher-NA objectives, thus making it the best choice for many biomedical applications.

For further verification of the limited-view problem in OR-PAM of biological tissues, numerical simulations were carried out on the cortical blood vessels in a mouse brain using both 3-photon microscopy and OR-PAM. The brain vasculature was first acquired using 3-photon microscopy with fluorescein isothiocyanate as the contrast agent [24], as shown in Figure 4A.

Using 3 representative regions that contain the penetrating vessels as the numerical targets (Figure 4B,E,H), we simulated the OR-PAM images with 0.1- and 0.3-NA

**FIGURE 4** Numerical simulation on the cortical vessels in a mouse brain. (A) Original image by 3-photon microscopy. The red rectangles mark the regions of interest. The projected depth in the  $y$  direction is 0.204 mm. (B), (E), (H) Original images of 3 sub-regions of interest acquired by 3-photon microscopy. (C), (F), (I) Simulated images of corresponding sub-regions acquired by OR-PAM with a 0.1-NA objective. The vessels marked by yellow arrows show poor visibility. (D), (G), (J) Simulated images of corresponding sub-regions acquired by OR-PAM with a 0.3-NA objective, showing that the penetrating vessels can be visualized better



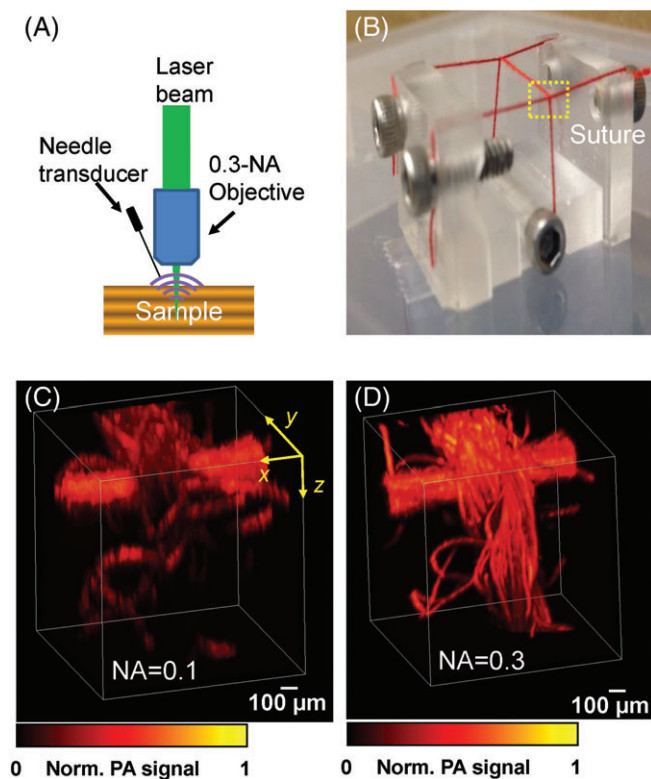


**FIGURE 5** Experimental validation of the limited-view phenomenon and the visibility improvement in OR-PAM. (A) Schematic of the OR-PAM system with a 0.3-NA water-immersion objective and a needle ultrasonic transducer. (B) Photograph of the suture phantom with 2 crossing parts. The dashed box marks the region imaged by OR-PAM. (C), (D) Volumetric OR-PAM image obtained with (C) a 0.1-NA objective and (D) a 0.3-NA objective, showing the improved visibility of the vertical structures with the high-NA objective

objectives. With the 0.1-NA objective, the horizontal vessels can be well imaged by OR-PAM, but the penetrating vessels are largely invisible, as shown in Figure 4C,F,I. This is because the DOF of the optical beam is relatively large and the acoustic waves from the penetrating vessels primarily propagate sideways and thus cannot be received by the ultrasonic transducer. In contrast, the visibility of the penetrating vessels is significantly improved with the 0.3-NA objective (Figure 4D,G,J) due to the much shorter DOF of the objective (Table 1), which is consistent with the results shown in Figure 3.

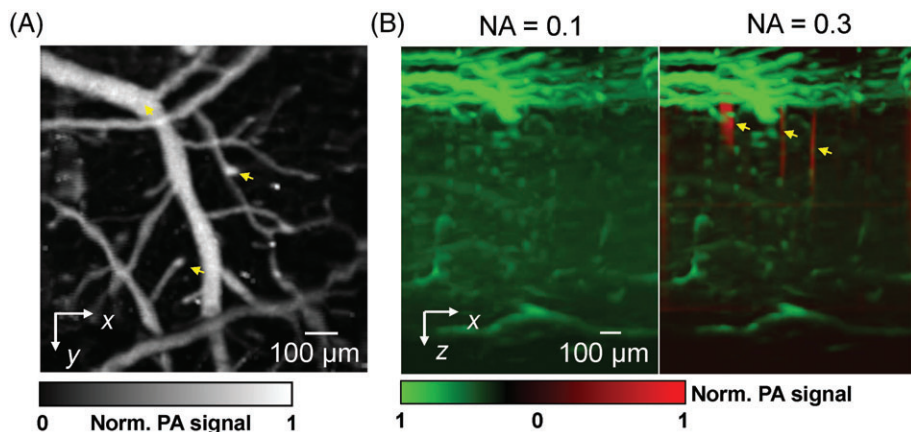


**FIGURE 6** Visibility improvement of OR-PAM in vivo. (A) An  $x$ - $y$  OR-PAM projection image of the mouse cortex with the scalp removed and skull intact. The arrows mark several representative diving vessels that are aligned with the acoustic axis (ie,  $z$  axis). (B) An  $x$ - $z$  projection image acquired by the OR-PAM systems with a 0.1-NA objective (left) and 0.3-NA objective (right), respectively. The diving vessels, as denoted by the arrows, can be imaged with the 0.3-NA objective but not the 0.1-NA objective. The diving vessels (shown in red) were segmented based on the difference of the 2 images

We imaged a suture-cross phantom to demonstrate the feasibility of improving the visibility of vertical structures by using a water-immersion objective with a 0.3 NA (UMPLFLN10XW(F), Olympus, Tokyo, Japan; working distance: 3.3 mm) (Figure 5A). To accommodate the short working distance of the objective, we used an unfocused needle ultrasonic transducer (diameter: 1 mm; central frequency: 40 MHz), which was placed in proximity to the objective ( $\sim 3$  mm to the optical focal plane) to receive the acoustic signals [25]. The acoustic axis of the transducer is about  $15^\circ$  from the optical axis of the objective, which can be approximated by the case shown in Figure 2B. The relatively low detection sensitivity of the needle transducer is partially compensated for because it is placed closer to the optical focus, compared with the traditional focused transducers. As a comparison, the same suture phantom was also imaged by the OR-PAM system with a 0.1-NA objective shown in Figure 1. The optical energy density was consistent under the 2 conditions. A  $z$  scanning with a step size of  $10 \mu\text{m}$  was performed for both objectives. The red suture phantom (Figure 5B) was imaged at 532 nm. The volumetric OR-PAM images with the 0.1- and 0.3-NA objectives (Figure 5C,D) clearly show that the 0.1-NA system was not able to receive the signals from the vertical structures of the suture-cross. In contrast, with the 0.3-NA objective, the visibility of the vertical structures was significantly improved, which is consistent with our numerical simulations above.

Finally, we performed in vivo mouse brain imaging with the scalp removed and the skull intact. The in vivo study was conducted on a female Swiss Webster mouse (10 weeks old and 32.1 g in weight) and the protocol was approved by the Institutional Animal Care and Use Committee (IACUC) of Duke University and described in our previous publication [7]. The same region of interest of the mouse brain (Figure 6A) was scanned using OR-PAM systems with a 0.1- and 0.3-NA objective, respectively. As expected, the diving blood vessels (or penetrating pia vessels), which were mostly parallel to the acoustic axis, were not visible in the 0.1-NA OR-PAM image, but were clearly imaged by the 0.3-NA OR-PAM (Figure 6B). We took the difference between the 2 images and segmented the diving

vessels, using our previous published method [26]. Briefly, we tracked the vessels in the 3-dimensional volumetric image starting from the brain surface. The diving vessels were identified with the least tortuosity along the  $z$  axis. These results strongly demonstrate the necessity of improved visibility of vertical structures in OR-PAM images.

#### 4 | CONCLUSION

In conclusion, we have for the first time established the existence the limited-view phenomenon in OR-PAM through numerical simulations and experimental validations. The results show that when a small-NA objective (eg, 0.1) is used in OR-PAM, the vertical structures cannot be detected due to the coherent signal generation and the relatively slow variance of the optical fluence along the acoustic axis. It is worth reiterating that this limited view problem with a low optical NA is unique to OR-PAM, which does not apply to other optical microscopy techniques, including confocal microscopy, 2-photon microscopy and optical coherence tomography. Nevertheless, OR-PAM still holds advantages in its superior sensitivity to optical absorption contrast and inherent depth resolution.

We have also demonstrated that the visibility of the vertical structures can be readily improved by using larger-NA objectives. Overall, a 0.3-NA objective, which is widely available, is sufficient to visualize the penetrating pia vessels in the mouse cortex, as shown by our numerical simulations and in vivo validations. To the general audience interested in using OR-PAM for their research, this work lays the theoretical and technical foundation for an effective and economical solution to the limited-view problem in OR-PAM.

#### ACKNOWLEDGMENTS

This work was supported by Duke MEDx fund to J.Y. We would like to thank Jun Xia and Mucong Li for useful discussions and experimental assistance.

#### Financial disclosures

None reported.

#### REFERENCES

- [1] L. H. V. Wang, J. J. Yao, *Nat. Methods* **2016**, *13*, 627.
- [2] L. H. V. Wang, S. Hu, *Science* **2012**, *335*, 1458.
- [3] D. Huang, E. A. Swanson, C. P. Lin, J. S. Schuman, W. G. Stinson, W. Chang, M. R. Hee, T. Flotte, K. Gregory, C. A. Puliafito, J. G. Fujimoto, *Science* **1991**, *254*, 1178.
- [4] F. Helmchen, W. Denk, *Nat. Methods* **2005**, *2*, 932.
- [5] X. D. Wang, Y. J. Pang, G. Ku, X. Y. Xie, G. Stoica, L. H. V. Wang, *Nat. Biotechnol.* **2003**, *21*, 803.
- [6] J. J. Yao, J. Xia, L. V. Wang, *Ultrason. Imaging* **2016**, *38*, 44.
- [7] J. J. Yao, L. D. Wang, J. M. Yang, K. I. Maslov, T. T. W. Wong, L. Li, C. H. Huang, J. Zou, L. V. Wang, *Nat. Methods* **2015**, *12*, 407.
- [8] C. Kim, C. Favazza, L. H. V. Wang, *Chem. Rev.* **2010**, *110*, 2756.
- [9] Z. J. Guo, L. Li, L. H. V. Wang, *Med. Phys.* **2009**, *36*, 4084.
- [10] X. L. Deán-Ben, D. Razansky, *Photoacoustics* **2016**, *4*, 133.
- [11] J. Gateau, T. Chaigne, O. Katz, S. Gigan, E. Bossy, *Opt. Lett.* **2013**, *38*, 5188.
- [12] B. Huang, J. Xia, K. Maslov, L. H. V. Wang, *J. Biomed. Opt.* **2013**, *18*, 110505.
- [13] L. Wang, G. Li, J. Xia, L. V. Wang, *Optica* **2015**, *2*, 307.
- [14] J. Yao, L. V. Wang, *Photoacoustics* **2014**, *2*, 87.
- [15] C. Zhang, K. Maslov, J. Yao, L. V. Wang, *J. Biomed. Opt.* **2012**, *17*, 116016.
- [16] C. Zhang, K. Maslov, L. H. V. Wang, *Opt. Lett.* **2010**, *35*, 3195.
- [17] C. Zhang, K. Maslov, S. Hu, R. M. Chen, Q. F. Zhou, K. K. Shung, L. H. V. Wang, *J. Biomed. Opt.* **2012**, *17*, 020501.
- [18] M. H. Xu, L. H. V. Wang, *Rev. Sci. Instrum.* **2006**, *77*, 041101.
- [19] O. Svelto, D. C. Hanna, *Principles of Lasers*, 5th ed (Springer, Berlin, 2010), **2010**, p. 1.
- [20] B. E. Treeby, B. T. Cox, *J. Biomed. Opt.* **2010**, *15*, 021314.
- [21] B. T. Cox, P. C. Beard, *J. Acoust. Soc. Am.* **2005**, *117*, 3616.
- [22] E. M. Strohm, M. J. Moore, M. C. Kolios, *Photoacoustics* **2016**, *4*, 36.
- [23] Z. Guo, L. Li, L. V. Wang, *Med. Phys.* **2009**, *36*, 4084.
- [24] N. G. Horton, K. Wang, D. Kobat, C. G. Clark, F. W. Wise, C. B. Schaffer, C. Xu, *Nat. Photonics* **2013**, *7*, 205.
- [25] H. S. Hsu, F. Zheng, Y. Li, C. Lee, Q. Zhou, K. Kirk Shung, *Appl. Phys. Lett.* **2012**, *101*, 24105.
- [26] S. Oladipupo, S. Hu, J. Kovalski, J. J. Yao, A. Santeford, R. E. Sohn, R. Shohet, K. Maslov, L. H. V. Wang, J. M. Arbeit, *Proc. Natl. Acad. Sci. U.S.A.* **2011**, *108*, 13264.

**How to cite this article:** Liu W, Zhou Y, Wang M, et al. Correcting the limited view in optical-resolution photoacoustic microscopy. *J. Biophotonics*. 2018;11:e201700196. <https://doi.org/10.1002/jbio.201700196>